11

# An Analysis of Blood Flow Dynamics in AAA

Bernad I. Sandor[1], Bernad S. Elena[2],
Barbat Tiberiu[1], Brisan Cosmin[2] and Albulescu Vlad[2]
[1]*Romanian Academy – Timisoara Branch,*
[2]*University of Medicine and Pharmacy "Victor Babes" Timisoara,*
*Romania*

## 1. Introduction

The current standard for determination of AAA disease progression is external aneurysm diameter measurement (Vainas et al., 2003), where the diameter enlargement is an indirect cumulative indicator of disease progression.
Generally, the maximum diameter and expansion rate of the AAAs, obtained from ultrasound or CT scans is used to assess the risk of rupture. Surgical treatment is recommended when the maximum diameter of AAA measures 55 mm or above (Katz & Cronenwett, 1994; Lederle et al., 2002).
The untreated AAAs, tend to grow and may rupture or dissect upon reaching a diameter of 6–7 cm (Katz & Cronenwett, 1994). At this stage, it is likely that the arterial wall will no longer withstand the blood pressure, and surgical intervention is usually recommended for aneurysms 0.5 cm below than the critical diameter (Lederle et al., 2002).
Various past numerical and experimental studies were conducted to investigate blood flow patterns in the AAAs. Disturbance in blood flow influence physiological parameters and processes, pressure, wall shear stress (WSS), wall remodelling and inflammation (Fillinger et al., 2003).
In this work we describe the complexity of the blood flow using a time dependent analisys, to determine the effects of aneurysm asymmetry, wall shear stress distribution and vortex dynamics inside the aneurysm.

## 2. Patient and methods

The study subject was male (62 year old), and the AAA maximum transverse diameter was 6.4 cm. The total length of the AAA was 11.6 cm. Patient-specific computed tomography (CT) scans were obtained, in order to investigate the AAAs' wall shear stress.

### 2.1 Anatomical model reconstruction

To produce a realistic three-dimensional model of a patient anatomy, spiral CT (Somatom Sensation 64 Scanner - Siemens Medical Systems, Erlangen, Germany) data was then used to reconstruct the infrarenal section of the aorta. The selected patient had an anterior-posterior asymmetric aneurysm in the infrarenal aorta with a maximum diameter of approximately 6.4 cm (Figure 1). Digital files in Digital Imaging and Communications in Medicine

(DICOM) file format, containing cross-sectional information were then imported to CFD software package for reconstruction.

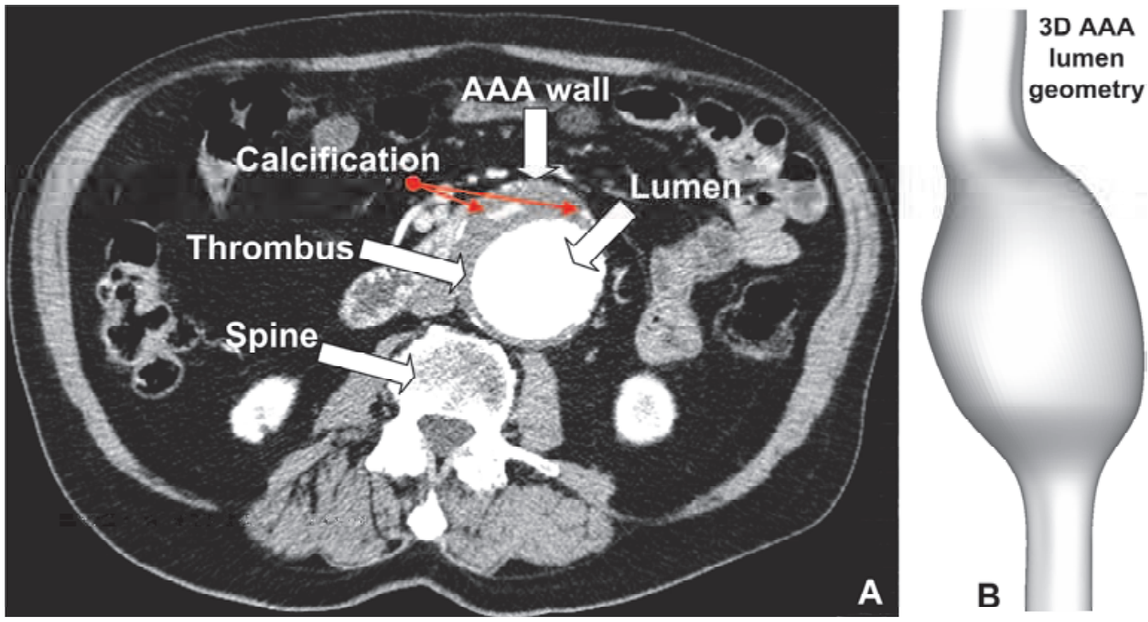


Fig. 1. CT scan and 3D reconstruction of the investigated section of the abdominal aorta. Axial cross-section CT slices are used for the three-dimensional reconstructions (A). 3D reconstruction of examined AAA (B). Anterior-posterior asymmetric AAA model result from the CT-scan.

The reconstructed aneurysm model is shown in Figure 2. The asymmetry parameter β (Figure 3) is defined as the ratio of the maximum posterior and anterior wall dimensions (Kleinstreuer & Vorp, 2006). Asymmetry parameter for the investigated patient are $\beta = 0.37$.

The corresponding finite-element computational domain is composed of 574,280 hexahedral linear elements, for a total of 596,181 nodes. The software Gambit v2.4 (Ansys Fluent, Ansys Inc., 2006) was used for the mesh generation (Figure 4).

A fine resolution near the wall, with the height of the wall boundary cells ($y+ < 2$) and a minimum of at least 7 grid nodes inside the boundary layer was ensured for the geometry owing to the requirements of the numerical model.

Mesh independence study we performed in order to determine the optimum number of mesh elements. The optimum mesh size was determined once the peak wall shear stress does not increase by more than 2%.

### 2.2 Boundary conditions

At the inlet, a spatial velocity profile was imposed (Figure 5). These waveforms are triphasic pulses appropriate for normal hemodynamics conditions in the infrarenal segment of the human abdominal aorta first reported by Mills (Mills et al., 1970). The use of an input transient velocity based on normal physiology is justified by the fact that the inlet boundary condition is applied in the section of undilated segment of the abdominal aorta anterior the proximal neck of the aneurysm (Finol et al., 2003).

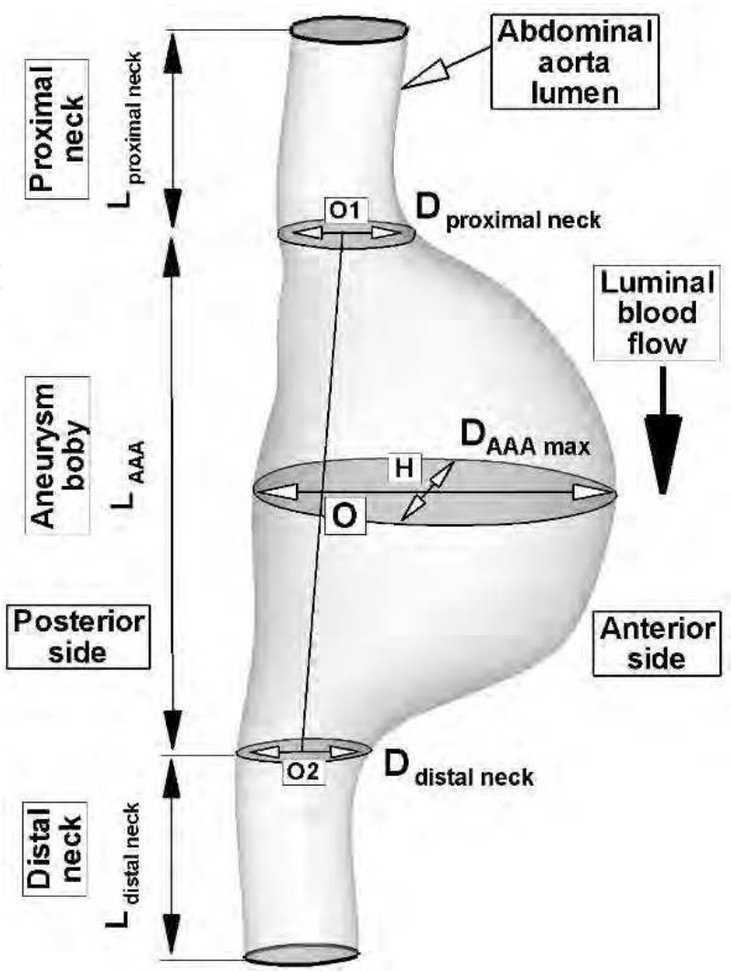


Fig. 2. Computational domain for asymmetry parameter β =0.37. Geometrical parameters used for AAA rupture risk evaluation.

In order to prevent overestimating the wall shear stress, a zero pressure state AAA has been used in present numerical simulations (Marra et al., 2005). No slip condition was applied at the fluid-wall interface. The cardiac cycle period was 1 s, with peak systolic flow occurring at 0.302s, and peak diastolic flow at 0.7s (Figure 5b). The length of the systolic and diastolic periods were 0.32s and 0.68s respectively. Blood was treated as a incompressible Newtonian fluid, an acceptable assumption for large arteries (Perktold et al., 1991).

Hemodynamic parameters are considered to be responsible for aneurysm initiation and growth. In majority of the computational studies, non Newtonian viscosity of blood, wall elasticity, blood particle composition and temperature effects are neglected, due to their secondary importance. The hemodynamic factors play a vital role in regulating the structure and functions of the endothelial layer.

We considered the dynamic viscosity of 0.004 Pas and density of 1050 kg/m3 for the blood (Table 1). The shear stress induced by blood flow was neglected in this study (Raghavan et al., 2000; Raghavan & Vorp, 2000; Thubricar et al., 2001), although the effects of blood flow have been shown to reduce wall stress by 10% in uniformly thick walled ideal models and by up to 30% in variable wall thickness models (Scotti et al., 2005).

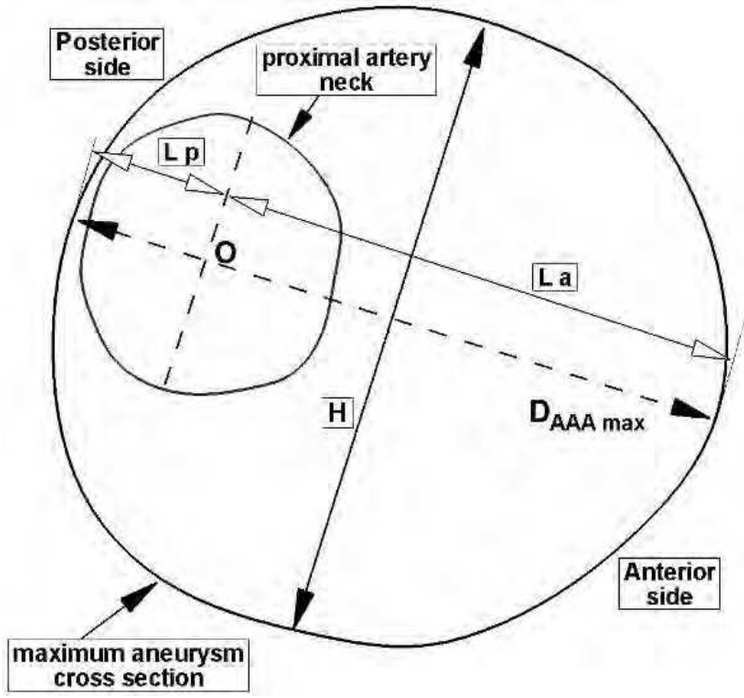


Fig. 3. Artery neck projected onto the plane of maximum aneurysm cross section.

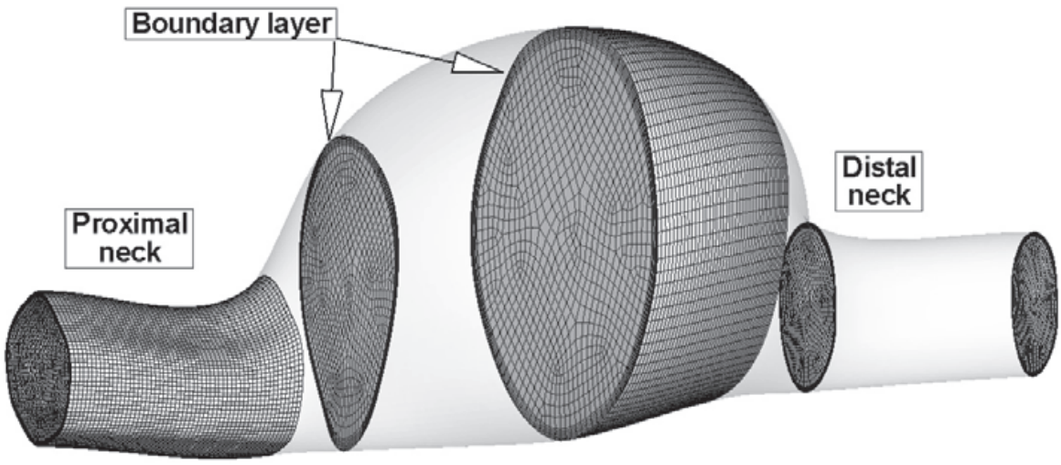


Fig. 4. Computational model for the patient specific reconstructed AAA. Intraluminal fluid mesh. Boundary layer contained 7 grid modes.

Incompressible, Newtonian flow is simulated for average resting conditions at a heart rate of 65 bpm. The governing equations are solved with the software Ansys FLUENT v6.3 (Ansys Inc.), which uses the finite volume method (FVM) for the spatial discretization. The workstations used to perform the simulations in this work is TYANPSC 600 (Tyan Computer Corporation) personal supercomputer with Intel® Xeon™ 5100 Dual Core, 40.0 GB RAM memory, and running on Windows® Compute Cluster Server 2003 operating system. The run time for a single simulation (on 8 processors) based on 3 consecutive pulsatile flow cycles was approximately 5 days real time.

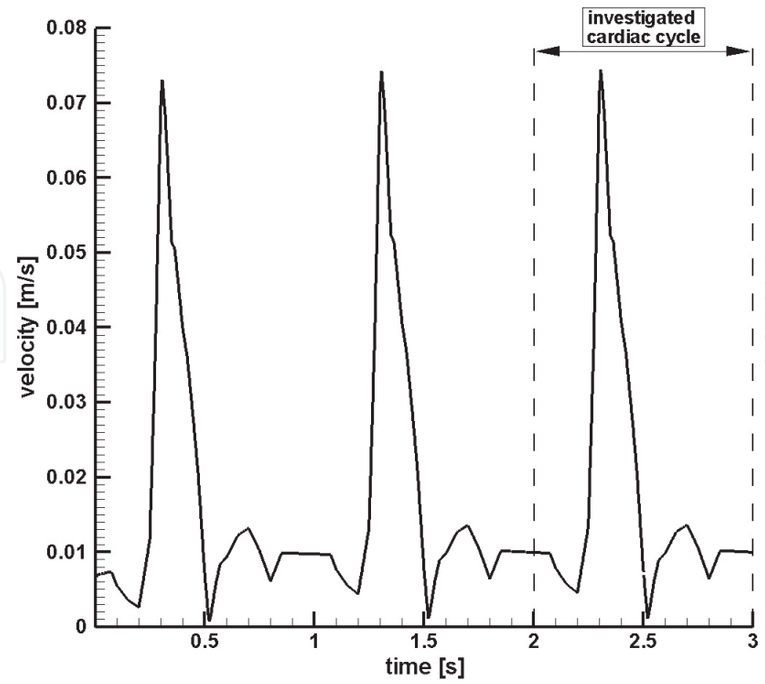


(a)

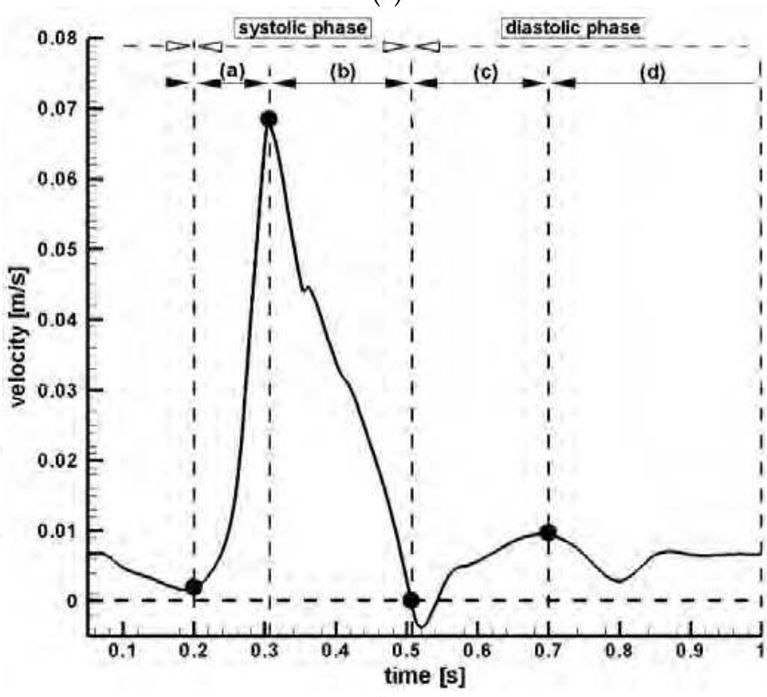


(b)

Fig. 5. Pulsatile velocity waveform reproduced from Scotti (Scotti et al., 2005). Enlarged view of the first three cardiac cycle (a). Peak systolic flow occurs at t=0.302 s and diastolic phase begins at t=0.52 s (b). In figure (b), we have: a - systolic acceleration, b - systolic deceleration, c - early diastole, d - late diastole.

| Parameters | Normal artery[a] | Aneurysm[b] | Current simulation |
|---|---|---|---|
| Wall thickness | 1.5 mm | 0.5-2.0 mm | 1.5 mm |
| Inner diameter | 20 mm | 40-80 mm | 30-64 mm |
| Length | Inlet: 200 mm<br>Outlet: 60 mm | 80 mm | 116 mm |
| Density | 1120 kg/m$^3$ | 1120 kg/m$^3$ | 1050 kg/m$^3$ |
| Others | | Asymmetry: $0.45 \le \beta \equiv L_p / L_a \le 1$ | Asymmetry: $\beta \equiv L_p / L_a \equiv 0.37$<br>(See Figure 4) |

[a]Reference (Raghavan & Vorp, 2000),
[b]Reference (Di Martino et al., 2001).

Table 1. Parameters used in the numerical simulation

## 3. Results

Based on the AAA pulsatile flow (Figure 5b), the following four flow phases summarize the aneurysm's size and the asymmetry parameter both dependent of the flow dynamics (Finol et al., 2003):

1. *Systolic acceleration* involves downstream ejection of the residual vortices.
2. *Systolic deceleration* is characterized by flow separation in the proximal neck.
3. *Early diastole* is characterized by reduced in size of flow recirculation.
4. *Late diastole* is characterized by recirculation regions present downstream of the aneurysm midsection.

### 3.1 Velocity profiles

Aneurysm sac diameter, aspect ratio, aneurysm shape and parent artery diameter are the parametric factors known to influence the nature of blood flow within an aneurysm. In CFD as well as in experimental studies, the researchers studied intra aneurismal flow as a function of these geometric parameters. For example, the neck size decide the amount of flow entering in the aneurysm sac and the volume of the aneurysm deciding on how sluggish the flow in the aneurysm sac.

The investigated AAAs demonstrates complex flow patterns over the cardiac cycle. The effect of aneurysm asymmetry in pulsatile flow dynamics is depicted in Figures 6, 7 and 8. At peak flow t=0.3s (Figure 6a), a characteristic attached flow pattern is obtained throughout the aneurysm with nearly stagnant flow, present along the anterior wall where the diameter is the greatest (cross-section B-B). During systolic deceleration, flow separation occurs and the vortex begins to travel in the aneurysm sac.

The complex flow pattern was observed at t=0.7s near the exit of the proximal neck of the aneurysm, where the flow is intensified and recirculation zones are present (Figure 7b). This stage is depicted with significant and asymmetric flow recirculation near the aneurysm proximal neck (Figure 7b, cross-section A-A).

In Figure 7, we see an internal jet of fluid surrounded by a recirculating vortex. At the end of the systolic deceleration phase, a small recirculating vortex develops at the end of the proximal neck. During systolic deceleration and early diastole a large recirculating flow region fills the aneurysm sac.

Figures 6 and 7 illustrates secondary velocity vectors in the cross section of the aneurysm. At the time t=0.3s near the proximal neck of the aneurysm exhibits no significant secondary flow, but one large secondary vortice is obtained along the proximal neck of the aneurysm at the time t=0.7 s (Figure 7b).
We can see in Figures 6, 7 and 8 the flow in investigated AAA presents two regimes. The first regime with no vortex formation is presented in Figures 6 and 8a, and the second regime is with vortical structures (Figures 7 and 8b). These flow regimes, depend on the different phases of the cardiac cycle and on the aspect ratio of the aneurysm.

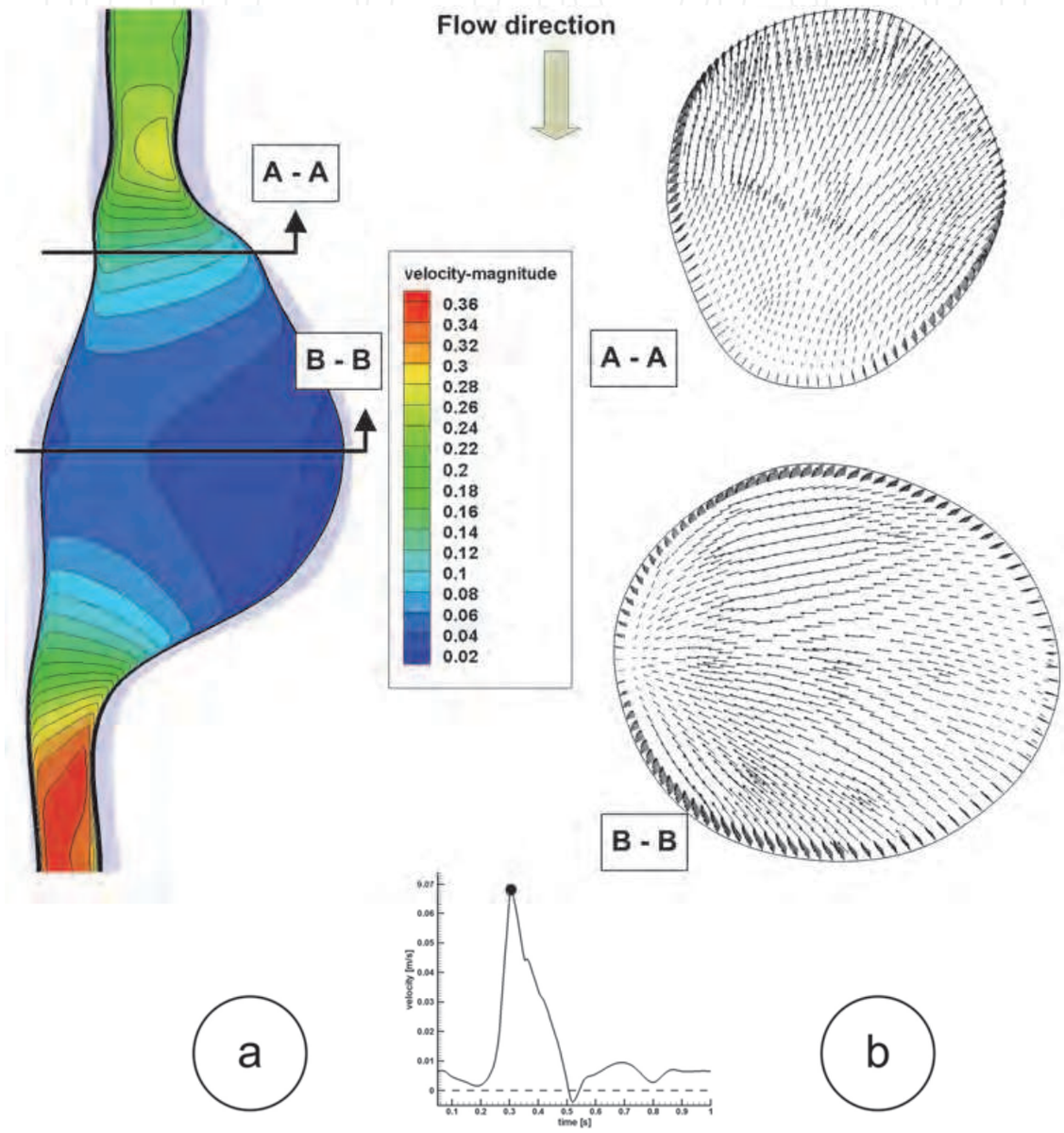


Fig. 6. Velocity field at the time t=0.3s, peak systole in the AAA. a) longitudinal section, velocity magnitude contour plot; b) velocity vector plot in cross-section; A-A in proximal neck and B-B in the maximum diameter region

The flow in the aneurysm decelerates and becomes unstable. This leads to flow separation, recirculation and possible transition to turbulence (Khanafer et al., 2007). Turbulence is induced by sudden expansion of the flow in the proximal neck (Figure 8b). This flow expansion generates recirculation region which produce additional wall shear stresses, increasing the rate of wall dilation (Khanafer et al., 2007).

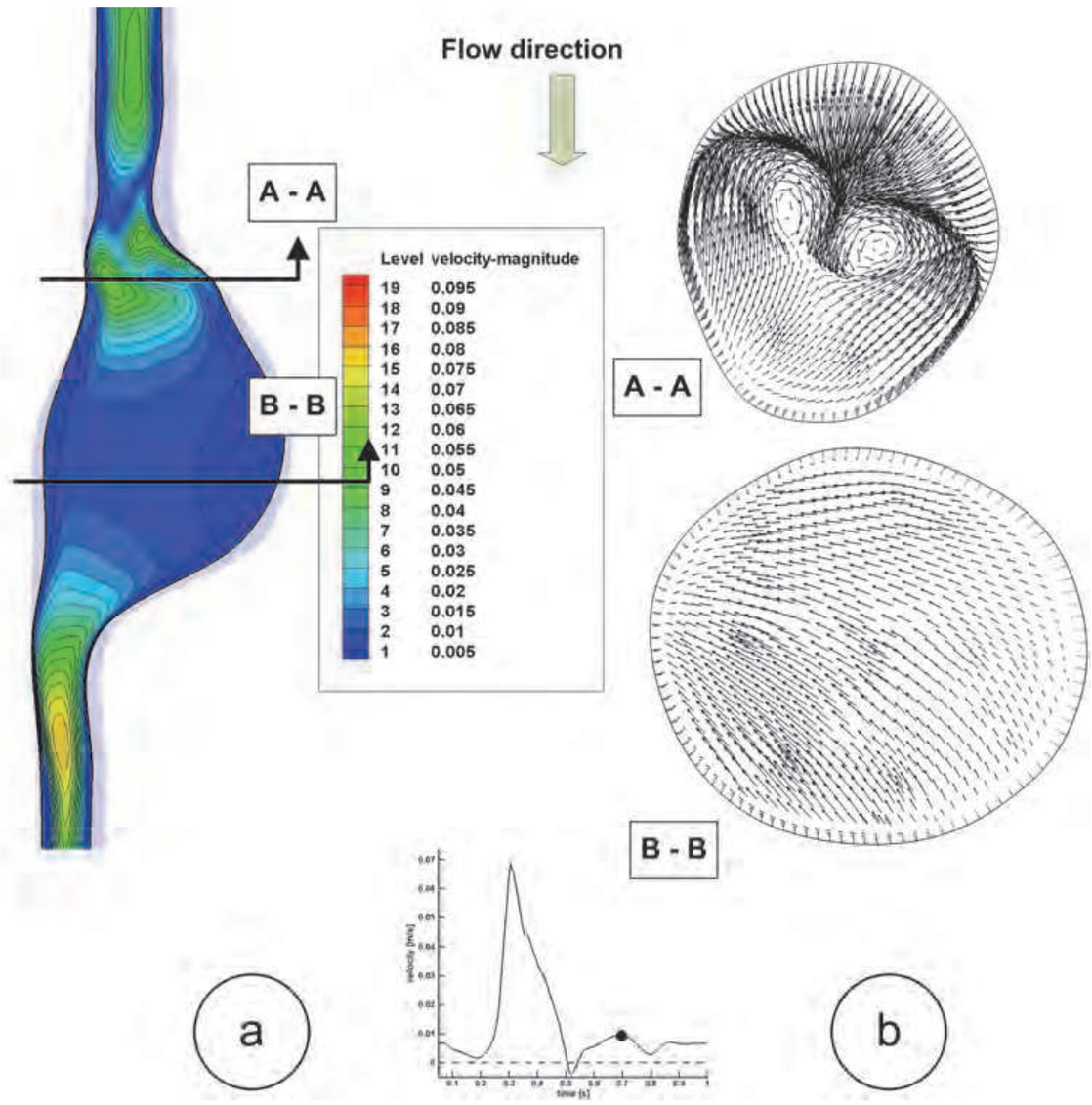


Fig. 7. Velocity magnitude b) Cross-section velocity vectors in proximal neck and maximum diameter region at the time t=0.7 s of the cardiac cycle. Vortical flow through the proximal neck.

### 3.2 Wall shear stress analysis

Throughout the cardiac cycle the wall shear stress distribution corresponds to the velocity gradients. Fluid shear stress is defined as a measure of the tangential forces per unit area generated by the flow stream on the walls of the AAA.

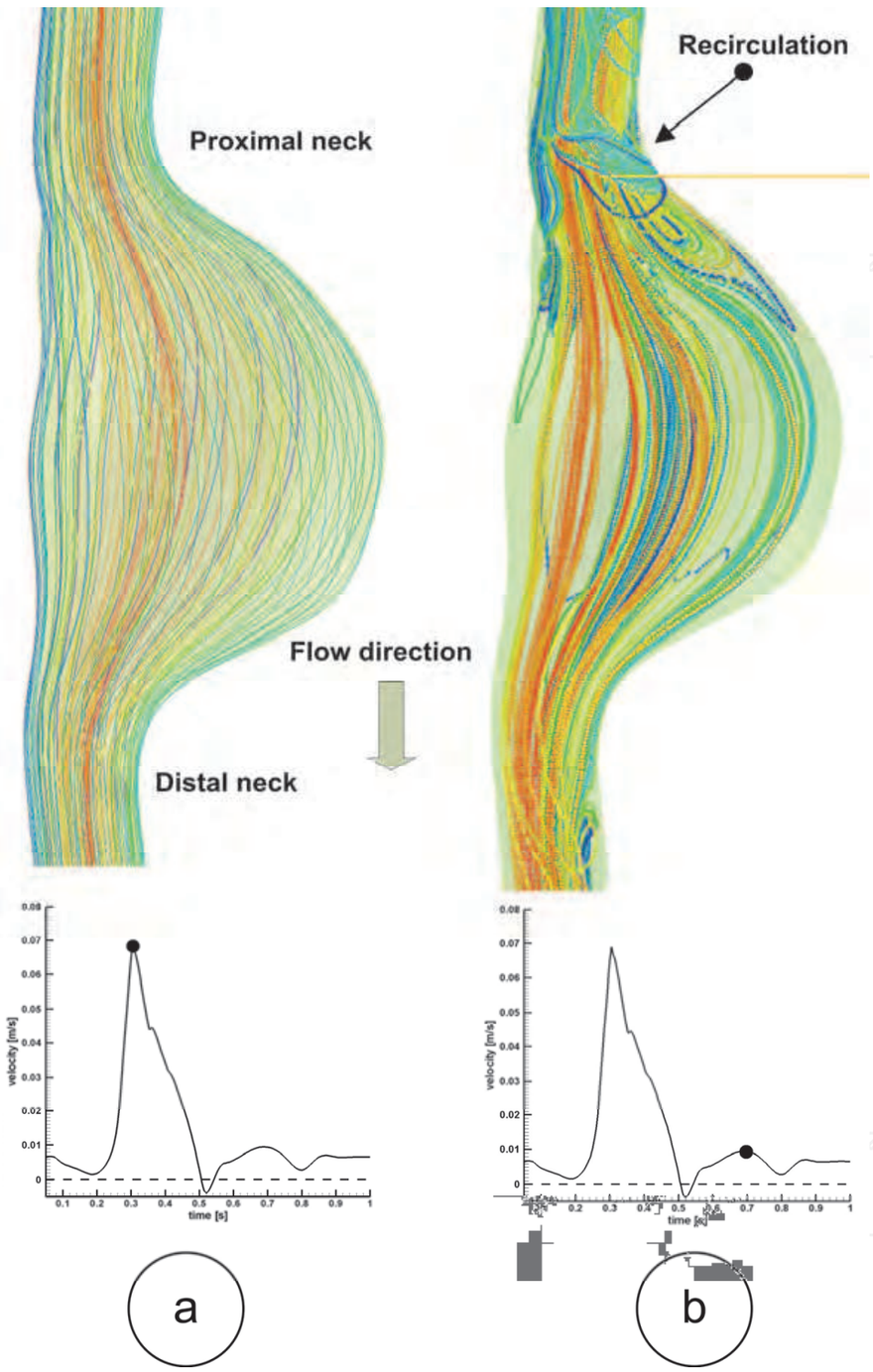


Fig. 8. a) 3D flow patern in the investigated AAA. b) Strong recirculation is present in the proximal neck and in the end of the distal neck. Helical flow is show inside to the aneurysm sac.

Along the maximum transversal diameter of the aneurysm, a slow recirculating flow exists, where the WSS is low. This flow pattern increase the residence time of blood along the aneurysm sac resulting in enhanced mass transfer.

Low wall shear stress in the range of ± 0.4 Pa plays a vital role in degenerating the endothelial layer, and resulting in an inflammatory cell response by initiating vascular wall remodeling (Malek 1999). We can see in Figure 9, that the WSS less than 0.4 Pa covered a wide area of the aneurysm body.
High WSS occurres in the proximal aneurysm neck, and low WSS in regions of flow separation (Figures 9 and 7). Sudden changes in cross-sectional area or in curvature cause local increment and adverse pressure gradient which creates low WSS in the aneurysm body (Figure 9). Regions of high WSS are likely to lead to matrix degradation by expression of plasmin, matrix-metalloproteinases and smooth muscle cells apoptosis (Ekaterinas et al., 2006). This may cause degenerative lesions of aneurysmal wall, altering the wall thickness and eventually causing rupture (Tan et al., 2008).

## 4. Discussion

Previous numerical studies in the literature, pointed that the flow in an aneurysm is complex with presence of vortices, secondary flows and strong amplification of instability (Venkatasubramaniam et al., 2004).
The velocity profiles showed highly disturbed flow and recirculation within the aneurysm sac. At the end of systole, the flow is a combination of rotational and recirculated secondary flows (Figures 7 and 8). Cross-sectional velocity profiles showed disturbed flow and recirculation in proximal neck region and in the aneurysm sac (Figure 7b).
During diastole the flow became instable and recirculation occurred almost everywhere in the aneurysm sac (Figure 8b). The flow patterns observed here, are characterized by helical flow and large recirculation zone. Same results found in literature for the blood flow in presence of the aneurysm (Tan et al., 2008; Boutsianis et al., 2009).
Disturbed flow induced by sudden expansion of the flow stream, results in additional stresses acting on the aneurysm wall that may be responsible for further aortic dilation. Dilation results in further radial expansion of the flow stream and in intensified turbulence. The latter then becomes a self-perpetuating mechanism for aneurysm dilation (Doyle et al., 2007).
Recirculation presented by the vector plot in aneurysm sac, suggested that certain disturbed flow conditions may cause injury to endothelium and induce stimuli for inflammation or degradation.
Consequently, complex flow pattern, by increasing wall tension may induce dilation of an aneurysm. Cyclic turbulent stresses are known to alter the structure and integrity of the arterial wall. Large eddies induce vibrations at frequencies which cause the dilation of arteries (Khanafer et al., 2007).
Due to the highly three-dimensional nature of blood flow in the abdominal aneurysm, it can be a difficult task to keep track of the paths of fluid particles within the flow field.
An effective way to investigate these fluid motions is to numerically inject a passive or non-interactive tracer into the flow, and we have carried out such an investigation in the present work. We have introduced a tracer, which serves as a visualization tool to analyze the flow characteristics. Figure 10 presents the tracer distribution inside to the aneurysm's body.
Further, in a large recirculating flow region the particles residence time is large and could be a contributing factor for thrombosis in the aneurysm.
The obtained results for WSS are in agreement with published data from the investigations considering the physiological aorta (Doyle et al., 2007) as well as with data from patient-specific fluid-solid interaction simulations (Leung et al., 2006).

Pressure contours at the peak systole (time t=0.3s) and peak diastole (t=0.7s) are presented in Figure 9. Pressure gradient generally decreases in the flow direction. Highest pressure of about 15.4 kPa (115.5 mmHg) at the time t=0.3s is found in the exit region of the AAA.
Therefore the highest pressure difference between inlet and outlet is about 1.3kPa (9.75 mmHg) at the time t=0.3s and about 0.6 kPa (4.5 mmHg) at the time t=0.7s . In diastolic flow, the inlet velocity begins to decelerate, reducing the overall pressure gradient.
As the cardiac cycle continues, pressure drop is expected to decrease and recirculation regions dominate of the aneurysm sac (Cheng et al., 2010).

### 4.1 Wall shear stress analysis

The blood flow dynamics in aneurysm models is governed by the compliance of the vessel. The velocity vectors illustrate a streamlined profile absent of vortices, a flow path customarily associated with a condition of systolic acceleration (Figure 8a).
The vortices are developed in the proximal neck and are dissipated in the aneurysm (Figure 8b). Vortex growth inside the AAA sac creates favorable conditions for increased platelet deposition rates and an increased risk of rupture (Thubrikar et al., 2003).
Geometry has been well established as a contributing factor to aneurysm expansion and rupture potential, independently of the heterogenity of the wall (Di Martino et al., 2001).
Significant gradients occur at the inflection points of the aneurysm curvature. For the investigated aneurysm, the changes in curvature lead to higher displacements and increased wall shear stress, suggestive for the effect of flow through the gradual expansions and contractions of the geometry (Figures 7 and 8).
Figures 7 and 9 present the area prone to vascular remodeling increases with decrease the blood velocity. In this case the flow along the aneurysm body is sluggish and the WSS along the maximum transversal diameter of the aneurysm drops, increasing the risk of leukocyte adhesion.

### 4.2 Study limitation

The study presented here is not without limitations. Firstly, it is known that calcifications occur in almost all AAAs. Intraluminal trombus - ILT and calcification were not included in the present study.
Another important limitation of the present study is the assumed uniform wall thickness. It has been shown that ILT can reduce the strain and the rate of dilation by up to 15% (Thubrikar et al., 2003).
The major assumptions used in the present study include the rigid wall approximation. These assumptions represent a reasonable first approximation for the blood flow in the abdominal aorta.

## 5. Conclusion

Based on a recent article describing how the aneurysm can induce a considerable increase in wall shear stress during flow systole in the region of aneurysm sac, we have used the CFD technique to investigate the relation between the blood hemodynamics and WSS during the cardiac cycle.

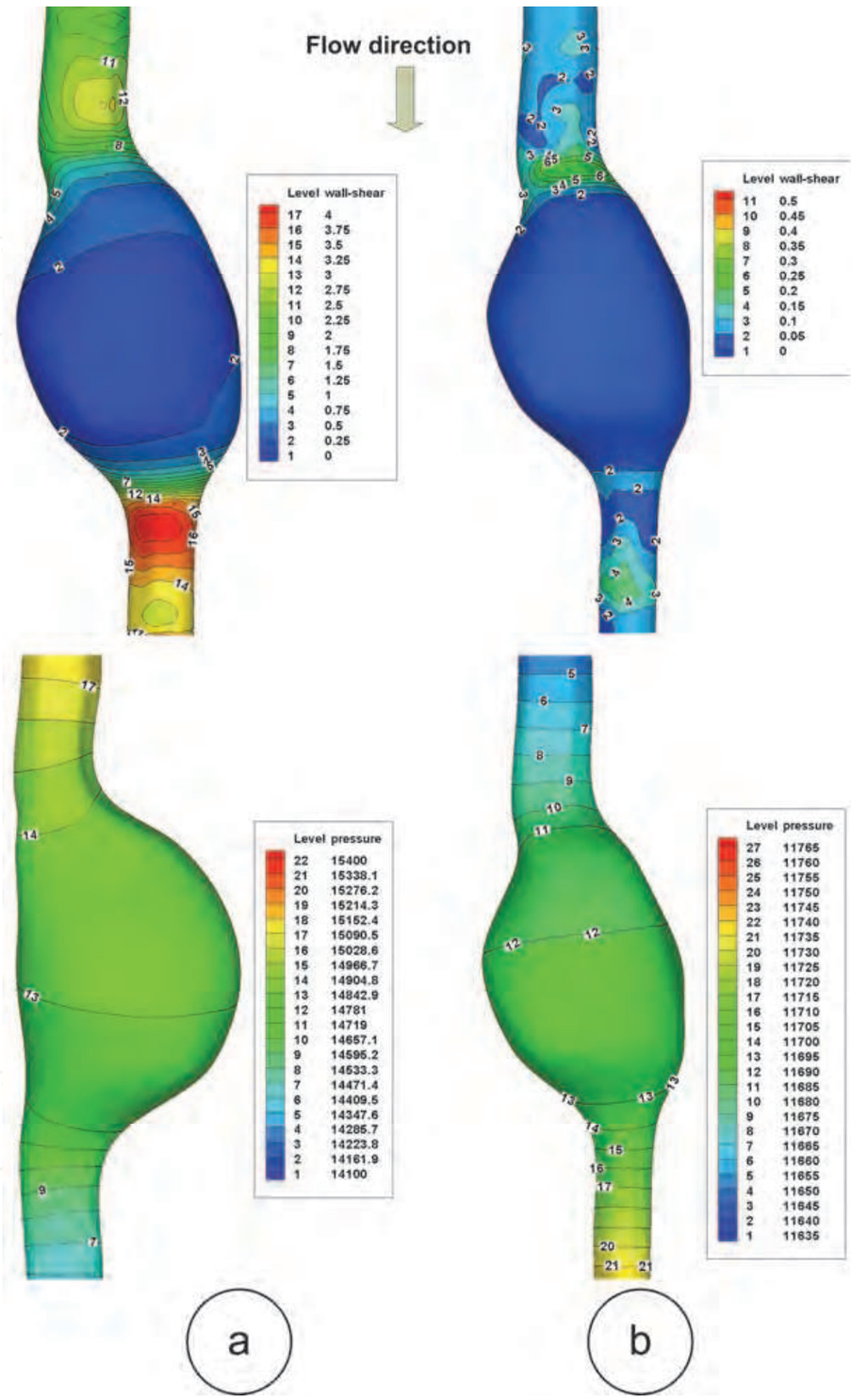


Fig. 9. Pressure and wall shear stress magnitude distributions on the anterior side of the aortic wall for different stages of the cardiac cycle: a) peak systole t=0.3 s and b) peak diastole t=0.7 s.

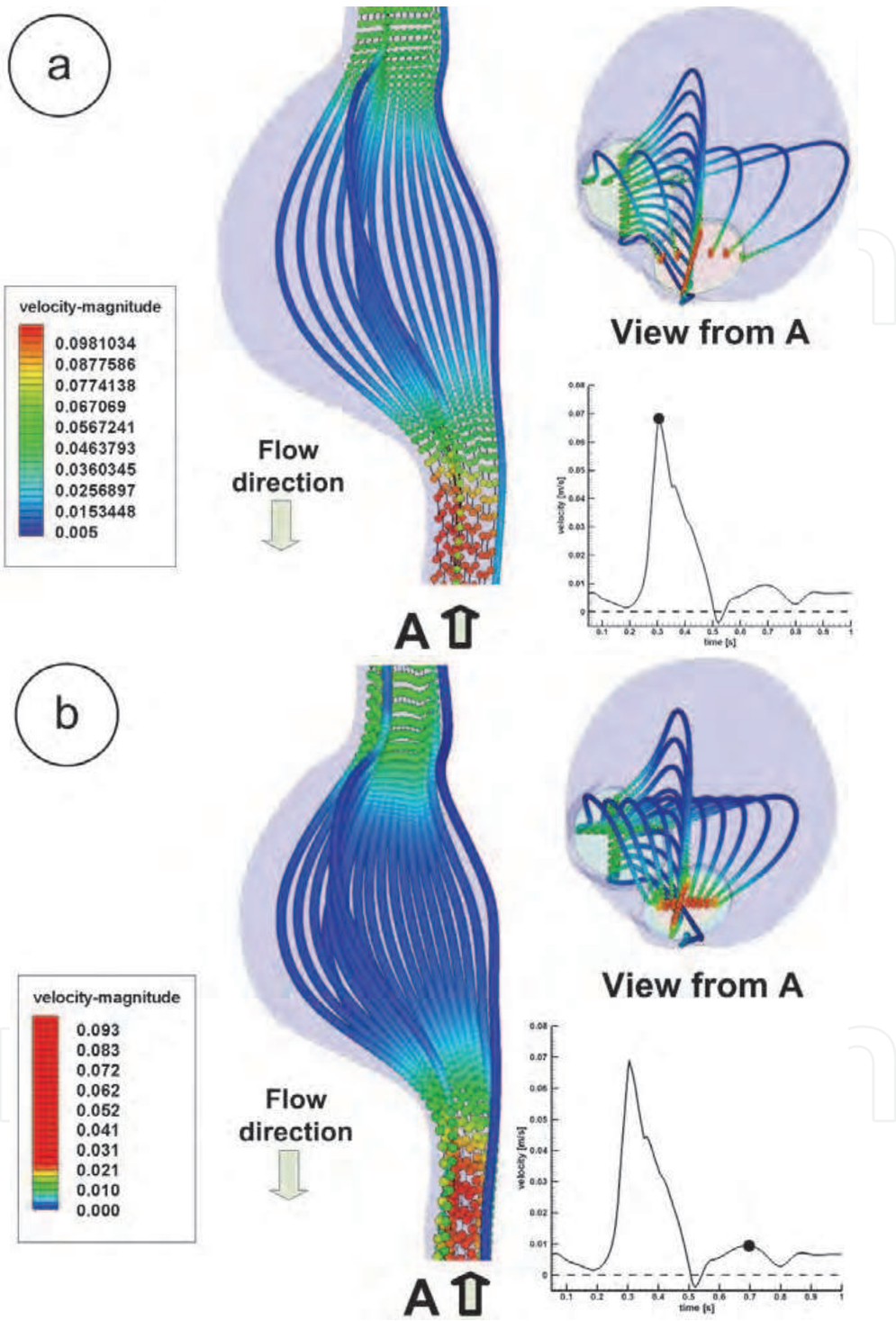


Fig. 10. Particles' motion inside the aneurysm colored by velocity magnitude at the different moment of the cardiac cycle: a) t=0.3 s and b) t=0.7 s. In order to compare the blood velocity in the different moment of the cardiac cycle, both velocity fields are represented for the same velocity range.

The virtual AAA models presented in this work provide a fundamental baseline for application of the CFD methodology as a non-invasive tool for rupture risk prediction in individual patients, outlining the importance of aneurysm asymmetry. This approach takes into account blood flow dynamics, which is inherently transient, and its effect on the wall mechanics. The present study demonstrates the relationship between the fluid velocity field and the flow-induced wall stresses. During the cardiac cycle, the instantaneous fluid forces acting on the inner wall will deform and expand the artery. From this study result that a complete understanding of the variation of intra aneurysmal hemodynamics with variations in the cardiac cycle is a critical tool for physician.

The fluid dynamics in a asymmetric aneurysm model is characterized by the development of vortices during the systolic deceleration phases. The distortion energy stored in the vessel as it expands during the cardiac cycle contributes to the early formation of recirculation regions in the aneurysm. This yields high velocity gradients at the distal end of the aneurysm. These flow patterns, in combination with the geometrical features of the model, determine the distribution of flow-induced wall stresses.

## 6. Acknowledgment

The present research has been supported by the Romanian National Authority for Scientific Research through the CNCSIS 798/2008 project, contract no: 590/2009.

## 7. References

Ansys FLUENT, Ansys Inc., User guide, 2006.

Boutsianis, E.; Guala, M.; Olgac, U.; Wildermuth, S.; Hoyer, K.; Venticos, Y. & Poulikakos, D. (2009). CFD and PTV steady flow investigation in an anatomically accurate abdominal aortic aneurysm. *Journal of Biomechanical Engineering*, Vol.131, p. 011008-15.

Cheng, Z.; Tan, F.P.P.; Riga, C.V.; Bicknell, C.D.; Hamady, M.S.; Gibbs, R.G.J.; Wood, N.B. & Xu, X.Y. (2010). Analysis of flow patterns in a patient-specific aortic dissection model. *Journal of Biomechanical Engineering,* Vol.132, No.5, 051007.

Di Martino, E.S.; Guadagni, G.; Fumero, A.; Ballerini, G.; Spirito, R.; Biglioli, P. & Redaelli, A. (2001). Fluid-Structure Interaction Within Realistic Three-Dimensional Models of the Aneurysmatic Aorta as a Guidance to Assess the Risk of Rupture of the Aneurysm. *Med. Eng. Phys.*, Vol.23, p. 647–655.

Doyle, B.J.; Callanan, A. & McGloughlin, T.M. (2007). A comparison of modelling techniques for computing wall stress in abdominal aortic aneurysms. *BioMedical Engineering OnLine*, Vol.6, doi:10.1186/1475-925X-6-38.

Ekaterinaris, J.A.; Ioannou, C.V. & Katsamouris, A.N. (2006). Flow dynamics in expansions characterizing abdominal aorta aneurysms. *Ann Vasc Surg*, Vol.20, No.3, pp.351–359.

Fillinger, M.F.; Marra, S.P.; Raghavan, M.L. & Kennedy, F.E. (2003). Prediction of rupture risk in abdominal aortic aneurysm during observation: wall stress versus diameter. *J Vasc Surg*, Vol.37, No.4, pp. 724–732.

Finol, E.A.; Keyhani, K. & Amon, C.H. (2003). The effect of asymmetry in abdominal aortic aneurysms under physiologically realistic pulsatile flow conditions. *Journal of Biomechanical Engineering*, Vol.125, pp. 207-217 .

Lederle, A.; Wilson, S.E.; Johnson, G.R.; Reinke, D.B.; Littooy, F.N.; Acher, C.W.; Ballard, D.J.; Messina, L.M.; Gordon, I.L.; Chute, E.P.; Krupski, W.C.; Busuttil, S.J.; Barone, G.W.; Sparks, S.; Graham, L.M.; Rapp, J.H.; Makaroun, M.S.; Moneta, G.L.; Cambria, R.A.; Makhoul, R.G.; Eton, D.; Ansel, H.J.; Freischlag, J.A. & Bandyk, D. (2002). Immediate repair compared with surveillance of small abdominal aortic aneurysms. *N Engl J Med*, Vol.346, No.19, pp. 1437-1444.

Leung, J.H.; Wright, A.R.; Cheshire. N.; Crane, J.; Thom, S.A.; Hughes, A.G. & Xu, Y. (2006). Fluid structure interaction of patient specific abdominal aortic aneurysms: a comparison with solid stress models, *BioMedical Engineering OnLine*, Vol.5. p. 33.

Katz, D.A. & Cronenwett, J.L. (1994). The cost-effectiveness of early surgery versus watchful waiting in the management of small abdominal aortic aneurysms. *Journal of Vascular Surgery*, Vol.19, pp. 980-990.

Kleinstreuer C. & Zhonghua L. (2006). Analysis and computer program for rupture-risk prediction of abdominal aortic aneurysms, *BioMedical Engineering OnLine*, Vol.5, p:19.

Khanafer, K.M.; Bull, J.L.; Upchurch, G.R. Jr.; Berguer, R. & Arbor, A. (2007). Turbulence Significantly Increases Pressure and Fluid Shear Stress in an Aortic Aneurysm Model under Resting and Exercise Flow Conditions. *Ann Vasc Surg.*, Vol.21, p. 67-74.

Malek, A.M.; Alper, S.L. & Izumo, S. (1999). Hemodynamic shear stress and its role in atherosclerosis. *Journal of the American Medical Association*, Vol.282, No.21, pp. 2035.

Marra, S.P.; Raghavan, M.L.; Whittaker, D.R.; Fillinger, M.F.; Chen, D.T.; Dwyer, J.M.; Tsapakos, M.J. & Kennedy, F.E. (2005). Estimation Of The Zero-Pressure Geometry Of Abdominal Aortic Aneurysms From Dynamic Magnetic Resonance Imaging. *Proceedings of the ASME 2005 Summer Bioengineering Conference,* Vail, Colorado, USA, June 22 – 26, 2005.

Mills, C.; Gabe, I.; Gault, J.; Mason, D. & Ross, JJr.; Braunwald, E. & Shillingford, J. (1970). Pressure-flow relationships and vascular impedance in man. *Cardiovascular Research*, Vol.4, pp. 405-417.

Perktold, K.; Resch, M. & Florian, H. (1991). Pulsatile non-Newtonian flow characteristics in a three-dimensional human carotid bifurcation model. *J Biomech Eng*, Vol.113, No.4, pp. 464-475.

Raghavan, M.L.; Vorp, D.A.; Federle, M.P.; Makaroun, M.S. & Webster, M.W. (2000). Wall stress distribution on three-dimensionally reconstructed models of human abdominal aortic aneurysm. *J Vasc Surg*, Vol.31, pp. 760-769.

Raghavan, M.L. & Vorp, D.A. (2000). Toward a Biomechanical Tool to Evaluate Rupture Potential of Abdominal Aortic Aneurysm: Identification of a Finite Strain Constitutive Model and Evaluation of its Applicability. *J. Biomech.*, Vol.33, p. 475–482.

Scotti, C.M.; Shkolnik, A.D.; Muluk, S.C. & Finol, E. (2005). Fluid-structure interaction in abdominal aortic aneurysms: effect of asymmetry and wall thickness. *Biomed Eng Online*, Vol.4, p: 64.

Tan, F.P.P.; Borghi, A.; Mohiaddin, R.H.; Wood, N.B.; Thom, S. & Xu, X.Y. (2008). Analysis of flow patterns in a patient-specific thoracic aortic aneurysm model. *Comput Struct*, doi:10.1016/j.compstruc.2008.09.007.

Thubrikar, M.J.; Robicsek, F.; Labrosse, M.; Chervenkoff, V. & Fowler, B.L. (2003). Effect of thrombus on abdominal aortic aneurysm wall dilation and stress. *J Cardiovasc Surg*, Vol.44, No.1, p. 67-77.

Thubrikar, M.J.; Al-Soudi, J. & Robicsek, F. (2001). Wall stress studies of abdominal aortic aneurysm in a clinical model. *Ann Vasc Surg*, Vol.15, pp. 355-366.

Vainas, T.; Lubbers, Y.; Stassen, F.R.M., *et al*. (2003). Serum C-reactive protein level is associated with abdominal aortic aneurysm size and may be produced by aneurysmal tissue. *Circulation*, Vol.107, pp. 1103–1105.

Venkatasubramaniam, A.K.; Fagan, M.J.; Mehta, T.; Mylankal, K.J.; Ray, B.; Kuhan, G.;, et al. (2004). Comparative study of aortic wall stress using finite element analysis for ruptured and non-ruptured abdominal aortic aneurysms. *Eur J Vasc Endovasc Surg*, Vol.28, No.2, pp. 168–176.

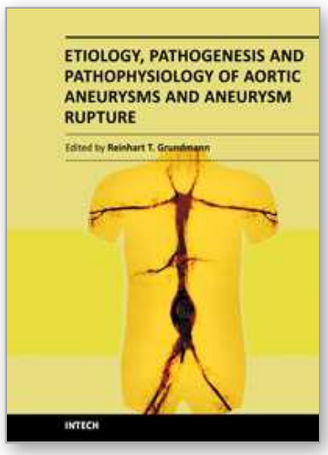


**Etiology, Pathogenesis and Pathophysiology of Aortic Aneurysms and Aneurysm Rupture**

Edited by Prof. Reinhart Grundmann

ISBN 978-953-307-523-5
Hard cover, 222 pages
**Publisher** InTech
**Published online** 27, July, 2011
**Published in print edition** July, 2011

This book considers mainly etiology, pathogenesis, and pathophysiology of aortic aneurysms (AA) and aneurysm rupture and addresses anyone engaged in treatment and prevention of AA. Multiple factors are implicated in AA pathogenesis, and are outlined here in detail by a team of specialist researchers. Initial pathological events in AA involve recruitment and infiltration of leukocytes into the aortic adventitia and media, which are associated with the production of inflammatory cytokines, chemokine, and reactive oxygen species. AA development is characterized by elastin fragmentation. As the aorta dilates due to loss of elastin and attenuation of the media, the arterial wall thickens as a result of remodeling. Collagen synthesis increases during the early stages of aneurysm formation, suggesting a repair process, but resulting in a less distensible vessel. Proteases identified in excess in AA and other aortic diseases include matrix metalloproteinases (MMPs), cathepsins, chymase and others. The elucidation of these issues will identify new targets for prophylactic and therapeutic intervention.

**How to reference**

In order to correctly reference this scholarly work, feel free to copy and paste the following:

Sandor Bernad, Elena-Silvia Bernad, Tiberiu Barbat, Cosmin Brisan and Vlad Albulescu (2011). An analysis of blood flow dynamics in AAA, Etiology, Pathogenesis and Pathophysiology of Aortic Aneurysms and Aneurysm Rupture, Prof. Reinhart Grundmann (Ed.), ISBN: 978-953-307-523-5, InTech, Available from: http://www.intechopen.com/books/etiology-pathogenesis-and-pathophysiology-of-aortic-aneurysms-and-aneurysm-rupture/an-analysis-of-blood-flow-dynamics-in-aaa

INTECH
open science | open minds

**InTech Europe**
University Campus STeP Ri
Slavka Krautzeka 83/A
51000 Rijeka, Croatia
Phone: +385 (51) 770 447
Fax: +385 (51) 686 166
www.intechopen.com

**InTech China**
Unit 405, Office Block, Hotel Equatorial Shanghai
No.65, Yan An Road (West), Shanghai, 200040, China
中国上海市延安西路65号上海国际贵都大饭店办公楼405单元
Phone: +86-21-62489820
Fax: +86-21-62489821

IntechOpen